Geochemical Perspectives Letters

Influence of metasomatism on vanadium-based redox proxies for mantle peridotite

A.B. Woodland, L. Uenver-Thiele, H.-M. Seitz

Supplementary Information

The Supplementary Information includes:

- Analytical Methods
- Oxybarometry based on Fe^{3+}-Fe^{2+} in Spinel and Clinopyroxene
- Bulk D_V for Peridotitic Compositions
- Tables S-1 and S-2
- Figures S-1 and S-2
- Supplementary Information References

Analytical Methods

EPMA

Major element compositions of clinopyroxene and other minerals necessary for computing oxidation state were measured with JEOL JXA-8900 superprobe and are reported in the supplementary tables of Uenver-Thiele *et al.* (2014). The analytical conditions are also detailed in that work.

LA-ICP-MS

Clinopyroxene trace element compositions were determined by LA-ICP-MS at the Goethe Universität Frankfurt (Germany). Clean clinopyroxene grains mounted in epoxy resin and polished were ablated with a Resolution M-50 (Resonetics) 193nm ArF excimer laser (ComPexPro 102F, Coherent) system. The ablation was performed with a 90 µm diameter spot size at 15 Hz and a laser power density of 6-7 J/cm^2. A helium stream (0.3 l/min) mixed with Ar as the sample gas with a flow rate of 0.85 l/min was used as carrier gas to the single collector sector field ICP-MS system (Element 2, ThermoFisher Scientific). Analyses were done in low-resolution mode, with an acquisition time of 20 s for background and 40 s for the sample. The oxide production rate was less than 0.5 % in order to suppress molecular interferences. The NIST 612 reference material and BIR glass served for external calibration and as secondary standard, respectively. Data processing was carried out with the GLITTER 4.4.2 software. The Si content of clinopyroxene, obtained from EPMA was used as an internal standard. Concentrations of Sc, V, Ga and Y as well as trace element ratios (V/Sc, La/Ce, Nd/Yb) are listed in Table S-1. Measured trace element concentrations for the BIR glass compared with published data indicates uncertainties of less than ±10 %. Additional trace element data are published in Uenver-Thiele *et al.* (2017).

Mössbauer Spectroscopy

Inclusion-free clinopyroxene grains were hand-picked under a microscope and ground into a fine powder in an agate mortar. A sufficient amount of clinopyroxene was used to produce an absorber thickness of ~5 mg Fe cm^{-2} to avoid potential saturation effects (Woodland *et al.*, 2006). The powder was mixed with a small amount of sugar (an Fe-free filler) to produce a sample without preferred orientation and packed into a pre-drilled hole in a 1mm thick Pb disc and closed off with tape.
Mössbauer spectra were obtained at room temperature operating in transmission geometry at a constant acceleration with a nominal 50 mCi 57Co source in a Rh matrix. The velocity scale was calibrated relative to 25-μm-thick α-Fe foil. Mirror-image spectra were collected over 512 channels using a velocity range of ± 5 mm/s. Clinopyroxene spectra are composed of two broad absorption peaks (Fig. S-1a, S-1b) and were fit following the spectral model described by Woodland *et al.* (2006), employing two quadrupole split doublets for Fe^{2+} and a single doublet for Fe^{3+}. The doublets had Lorentzian peak shapes and equal areas, although the relative peak widths of the Fe^{2+} doublets were allowed to vary in order to account for next-nearest-neighbour effects. In a few cases the quadrupole splitting of the Fe^{3+} doublet was fixed to 0.5 mm/s in order to obtain reasonable values for the isomer shift. Spectral fitting was performed using the NORMOS software package (Wissel Elektronik GmbH, Germany). Hyperfine parameters for the subspectra are provided in Table S-2, along with measured $Fe^{3+}/\Sigma Fe$. Uncertainties in $Fe^{3+}/\Sigma Fe$ are considered to be ± 0.01 (Woodland *et al.*, 2006). Fe^{3+} contents were determined by combining the obtained $Fe^{3+}/\Sigma Fe$ with total FeO measurements from EPMA.

Oxybarometry based on Fe^{3+}-Fe^{2+} in Spinel and Clinopyroxene

Spinel-based

The oxidation state of spinel peridotite is most often determined using the olivine-orthopyroxene-spinel equilibrium (*e.g.*, Wood *et al.*, 1990):

$$\underset{\text{olivine}}{6\,Fe_2SiO_4} + O_2 = \underset{\text{opx}}{3\,Fe_2Si_2O_6} + \underset{\text{spinel}}{2\,Fe_3O_4} \qquad \text{Eq. S-1}$$

which requires knowledge of the Fe^{3+} content (magnetite component) in spinel. $\Delta \log fO_2$ values based upon this equilibrium and referenced to the fayalite-magnetite-quartz (FMQ) oxygen buffer are listed in Supplementary Table S-1. These values are from Uenver-Thiele *et al.* (2014) and were computed assuming a constant pressure of 1.5 GPa, an equilibration temperature obtained from the two-pyroxene thermometer (Brey and Köhler, 1990) and activity models for spinel, olivine and orthopyroxene following Wood *et al.*, (1990). Overall uncertainties were estimated by Uenver-Thiele *et al.*, (2014) to be ±0.2-0.3 log units.

Clinopyroxene-based

Luth and Canil (1993) calibrated several olivine-orthopyroxene-clinopyroxene equilibria for estimating oxidation state based on the Fe^{3+} content of clinopyroxene. Their analysis indicated that the equilibrium:

$$\underset{\text{olivine}}{4\,Fe_2SiO_4} + \underset{\text{cpx}}{4\,NaAlSi_2O_6} + \underset{\text{cpx}}{2\,CaFe_2Si_2O_6} + O_2 = \underset{\text{cpx}}{4\,NaFe^{3+}Si_2O_6} + \underset{\text{cpx}}{2\,CaAl_2SiO_6} + \underset{\text{opx}}{3\,Fe_2Si_2O_6} \qquad \text{Eq. S-2}$$

along with the assumption of ideal mixing-on-sites in clinopyroxene yielded the most consistent results. This approach was taken here, following on its successful application by Woodland *et al.* (2006). Like for spinel, these calculations assumed a pressure of 1.5 GPa, along with equilibration temperatures given by orthopyroxene-clinopyroxene thermometry (Brey and Köhler, 1990). The Fe^{3+} contents of clinopyroxene were determined by Mössbauer spectroscopy, as described previously. The resulting $\Delta \log fO_2$ values are referenced relative to the FMQ buffer to be comparable with results from equilibrium (Eq. S-1) and are also listed in Table S-1. Luth and Canil (1993) assessed uncertainties to be ±0.8 log units.

Bulk D_V for Peridotitic Compositions

The fO_2-dependence of mineral/melt partitioning of V is summarised in Figure S-2 for all major peridotite phases following the experimental results of Mallmann and O'Neill (2009). Although these coefficients are valid for 1 bar, changing pressure should not influence the functional form of the fO_2-dependence (Mallmann and O'Neill, 2009; Li, 2018). Also plotted in Figure S-2 is the estimated fO_2-dependence of a bulk partition coefficient of V (D_V) pertinent for low-degree partial melting of a fertile peridotite containing 55 % olivine, 25 % orthopyroxene, 18 % clinopyroxene and 2 % spinel (Mallmann and O'Neill, 2009). It is apparent that the behavior of clinopyroxene mirrors that of the bulk, especially in the $\Delta \log fO_2$ range of FMQ-1 and FMQ+2 (shaded region), which likely reflects the conditions in the SCLM prior to and during interaction with the various metasomatising agents described by Uenver-Thiele *et al.* (2014).

Supplementary Tables

Table S-1 Selected trace element data for spinel peridotite xenoliths from the French Massif Central.

Table S-1 is available for download as an Excel file at http://www.geochemicalperspectivesletters.org/article1822.

Table S-2 Hyperfine parameters and $Fe^{3+}/\Sigma Fe$ for cpx.

Sample	Fe^{2+}			Fe^{2+}			Fe^{3+}			$Fe^{3+}/\Sigma Fe$	$\chi 2$
	IS	QS	FWHM	IS	QS	FWHM	IS	QS	FWHM		
1-LU3	1.13	2.10	0.49	1.01	2.59	0.44	0.49	0.50	0.60	0.284(12)	1.13
21-2	1.16	2.10	0.47	1.11	2.80	0.25	0.38	0.68	0.71	0.300(15)	1.03
22-7	1.13	2.07	0.47	1.11	2.77	0.34	0.46	0.53	0.69	0.274(19)	1.18
27-1	1.14	2.09	0.44	1.11	2.72	0.35	0.49	0.53	0.62	0.213(12)	1.26
27-2	1.14	2.10	0.44	1.11	2.62	0.29	0.52	0.49	0.55	0.174(11)	1.41
28-4	1.13	2.06	0.35	1.11	2.56	0.43	0.49	0.43	0.71	0.311(16)	1.45
28-5	1.12	2.10	0.42	1.09	2.62	0.40	0.51	0.57	0.56	0.283(14)	1.50
34-1	1.13	2.08	0.42	1.08	2.59	0.37	0.48	0.50	0.66	0.246(13)	1.38
39-1	1.14	2.03	0.35	1.09	2.32	0.53	0.52	0.50	0.62	0.254(14)	1.22
43-2	1.12	2.05	0.37	1.09	2.58	0.39	0.52	0.59	0.58	0.281(14)	1.10
44-LU3	1.13	2.06	0.39	1.08	2.48	0.39	0.52	0.50	0.59	0.247(15)	1.14
52-8	1.11	1.95	0.34	1.10	2.39	0.45	0.55	0.44	0.51	0.245(23)	1.01
55A-2	1.13	2.06	0.40	1.13	2.52	0.42	0.50	0.53	0.62	0.286(11)	1.20
60-1	1.14	2.07	0.40	1.14	2.57	0.45	0.46	0.62	0.52	0.291(10)	1.33
60-2	1.13	2.09	0.40	1.03	2.29	0.41	0.48	0.63	0.59	0.312(17)	1.00
61-2	1.12	2.04	0.41	1.13	2.59	0.40	0.48	0.44	0.66	0.257(25)	1.12
63-1	1.13	2.07	0.43	1.10	2.63	0.42	0.48	0.49	0.50	0.203(15)	1.10
64-1	1.13	2.08	0.45	1.12	2.64	0.32	0.53	0.49	0.50	0.171(12)	1.08
64-2	1.15	2.09	0.45	1.14	2.71	0.21	0.42	0.50	0.70	0.203(16)	1.06
71-2	1.13	1.90	0.38	1.15	2.30	0.47	0.40	0.50	0.79	0.241(19)	1.12
78-LU3b	1.13	1.84	0.39	1.17	2.20	0.53	0.34	0.57	0.78	0.197(29)	1.13
CON-A	1.15	2.10	0.53	1.11	2.67	0.08	0.43	0.65	0.68	0.329(17)	1.14
CON-B	1.12	1.98	0.40	1.13	2.39	0.50	0.47	0.50	0.67	0.268(18)	1.22
CON-D	1.13	2.08	0.42	1.09	2.57	0.39	0.54	0.47	0.50	0.185(13)	1.25
LA-A	1.14	1.97	0.39	1.13	2.31	0.47	0.40	0.69	0.71	0.308(21)	1.01
LA-F	1.14	2.04	0.42	1.09	2.54	0.43	0.46	0.64	0.71	0.258(15)	1.06
LEs1	1.12	2.07	0.41	1.11	2.57	0.46	0.50	0.56	0.58	0.260(8)	1.30
LEs2	1.13	2.09	0.43	1.12	2.62	0.35	0.54	0.50	0.52	0.212(8)	1.23
LEs3	1.13	2.08	0.45	1.11	2.64	0.37	0.51	0.45	0.56	0.198(9)	1.56
LEs4	1.12	2.04	0.39	1.13	2.47	0.44	0.52	0.51	0.56	0.249(8)	1.43
LEs5	1.14	2.03	0.43	1.13	2.53	0.47	0.47	0.53	0.70	0.254(10)	1.57
LEs6	1.13	2.09	0.45	1.10	2.72	0.36	0.53	0.51	0.60	0.220(9)	1.30
MB-B	1.15	1.96	0.37	1.10	2.30	0.49	0.48	0.50	0.72	0.228(24)	1.13
MB-B	1.16	1.99	0.45	1.17	2.47	0.26	0.32	0.86	0.69	0.231(21)	1.13
MBAR-A	1.13	2.10	0.46	1.10	2.61	0.31	0.48	0.50	0.66	0.256(21)	1.12
MBo-E	1.12	2.05	0.45	1.11	2.57	0.43	0.52	0.56	0.60	0.260(9)	1.23
MC-B	1.16	2.02	0.45	1.12	2.76	0.28	0.39	0.68	0.79	0.330(23)	0.95
MC-C	1.14	2.01	0.46	1.14	2.58	0.36	0.47	0.43	0.74	0.233(17)	1.13
MC-D	1.13	2.01	0.46	1.17	2.49	0.42	0.44	0.50	0.86	0.338(21)	1.10
MC-E	1.15	2.03	0.45	1.15	2.75	0.23	0.39	0.78	0.23	0.176(22)	1.04
MP-D	1.13	2.06	0.42	1.08	2.50	0.53	0.50	0.50	0.67	0.296(20)	0.94
MPS-B	1.13	2.06	0.38	1.12	2.50	0.37	0.49	0.37	0.65	0.273(15)	1.22
RdL-A	1.13	1.95	0.40	1.14	2.41	0.50	0.48	0.54	0.60	0.261(16)	1.16
RdL-B	1.13	2.05	0.45	1.13	2.54	0.34	0.51	0.60	0.62	0.318(17)	1.22
RdL-C	1.11	1.98	0.37	1.14	2.40	0.49	0.50	0.52	0.71	0.314(20)	1.13
Ri-A	1.13	2.10	0.41	1.10	2.60	0.40	0.53	0.56	0.62	0.302(13)	1.07

Supplementary Figures

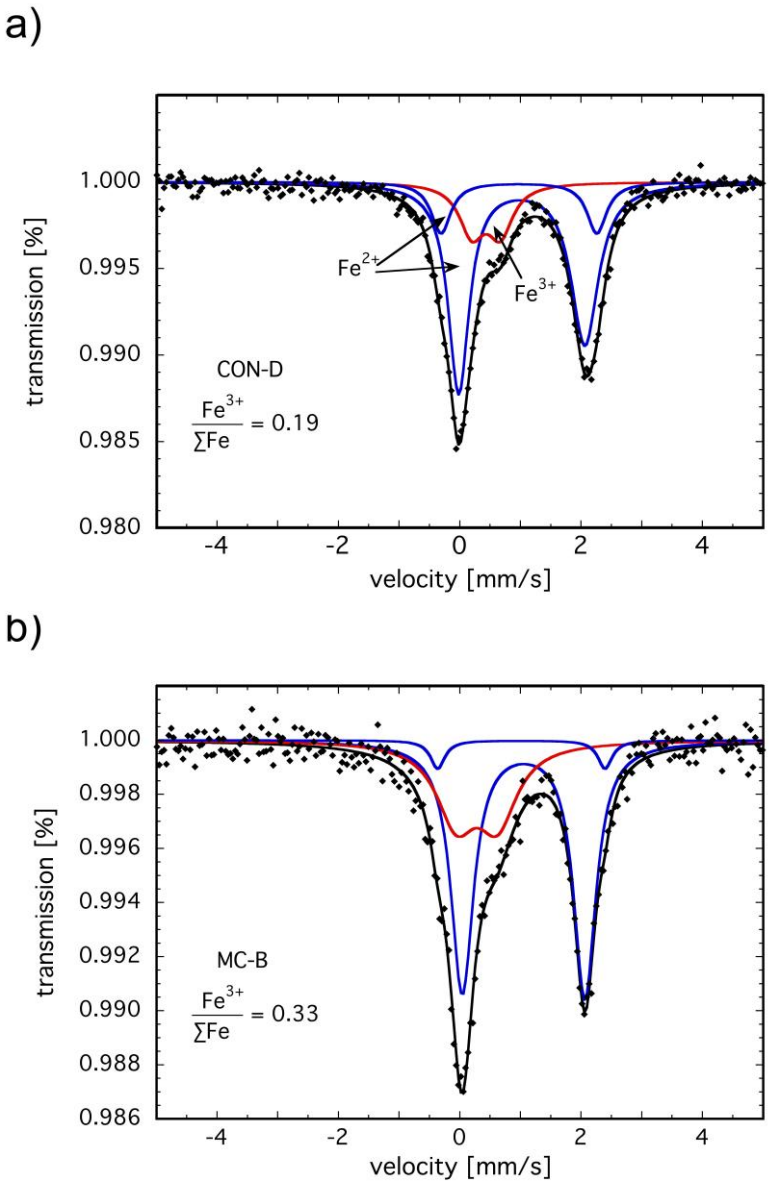

Figure S-1 Mössbauer spectra of clinopyroxene from samples **(a)** CON-D and **(b)** MC-B illustrating the range in Fe^{3+} contents observed in the xenolith suite.

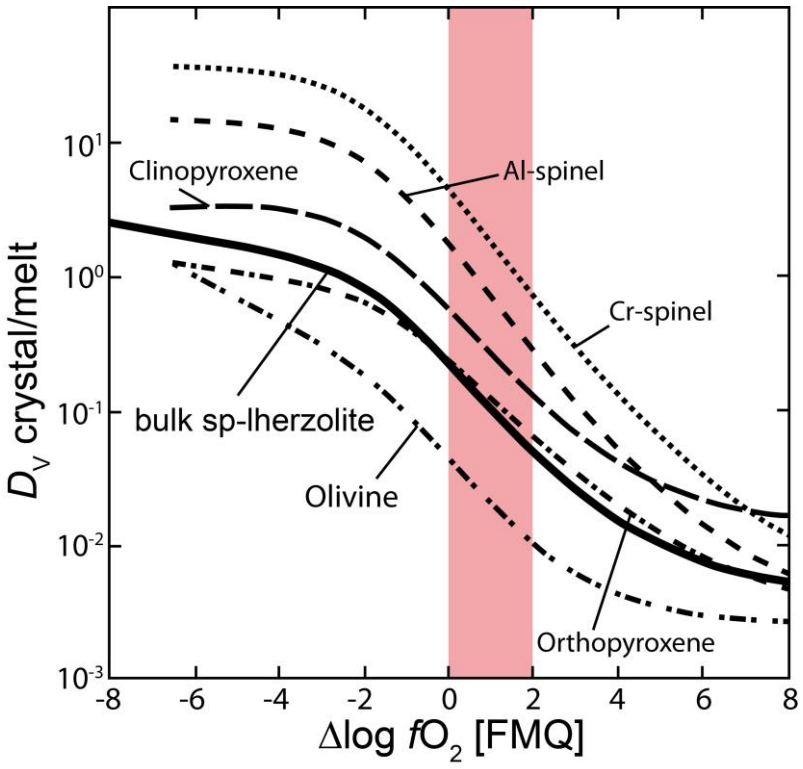

Figure S-2 Summary of experimentally determined mineral/melt D_V as a function of fO_2 at 1 bar for the major minerals in peridotite (olivine, orthopyroxene, spinel and clinopyroxene) and the resulting bulk/melt D_V estimated for partial melting of a fertile peridotite composition (Mallmann and O'Neill, 2009). The shaded region indicates the pertinent range in fO_2 for metasomatic interactions observed in our peridotites.

Supplementary Information References

Brey, G.P., Köhler, T. (1990) Geothermobarometry in four-phase lherzolites II. New thermobarometers, and practical assessment of existing thermobarometers. *Journal of Petrology* 31, 1353-1378.

Li, Y. (2018) Temperature and pressure effects on the partitioning of V and Sc between clinopyroxene and silicate melt: Implications for mantle oxygen fugacity. *American Mineralogist* 103, 819-823.

Luth, R.W., Canil, D. (1993) Ferric iron in mantle-derived pyroxenes and a new oxybarometer for the mantle. *Contributions to Mineralogy and Petrology* 113, 236-248.

Mallmann, G., O'Neill, H.St.C. (2009) The Crystal/Melt Partitioning of V during Mantle Melting as a Function of Oxygen Fugacity Compared with some other Elements (Al, P, Ca, Sc, Ti, Cr, Fe, Ga, Y, Zr and Nb). *Journal of Petrology* 50, 1765-1794.

Uenver-Thiele, L., Woodland, A.B., Downes, H., Altherr, R. (2014) Oxidation state of the lithospheric mantle below the Massif Central, France. *Journal of Petrology* 55, 2457-2480.

Uenver-Thiele, L., Woodland, A.B., Seitz, H.-M., Downes, H., Altherr, R. (2017) Metasomatic processes revealed by trace element and redox signatures of the lithospheric mantle beneath the Massif Central, France. *Journal of Petrology* 58, 395-422.

Wood, B.J., Bryndzia, L.T., Johnson, K.E. (1990) Mantle oxidation state and its relation to tectonic environment. *Science* 248, 337-345.

Woodland, A.B., Kornprobst, J., Tabit, A. (2006) Ferric iron in orogenic lherzolite massifs and controls of oxygen fugacity in the upper mantle. Lithos 89, 222-241.